

# xModel-KD: Cross-modal Knowledge Distillation for 3D Scene Perception using LiDAR

Thenukan Pathmanathan  
Dept. of Computer Science  
Lakehead University  
Thunder Bay, Canada  
tpathma1@lakeheadu.ca

Kanchan Keisham  
School of Computer Science Engg. & Info. Systems  
Vellore Institute of Technology  
Tamil Nadu, India  
kanchankeisham@gmail.com

Akilan Thangarajah  
Dept. of Software Engg.  
Lakehead University  
Thunder Bay, Canada  
takilan@lakeheadu.ca

**Abstract**—Point cloud segmentation is a fundamental task in 3D scene understanding. Its progress is constrained by the high cost and time required for dense 3D annotations, making labeled samples difficult to obtain. Beyond annotation scarcity, different sensing modalities face inherent limitations. 2D images provide rich texture and appearance cues, yet they lack explicit depth and geometric structure. In contrast, 3D point clouds capture accurate spatial geometry but are sparse and contain no texture information. As a result, relying on a single modality restricts the richness of learned representations and weakens generalization. Although recent multi-modal methods that combine 3D point clouds with 2D images have demonstrated strong performance in tasks such as classification and retrieval, they typically depend on large-scale labeled datasets and have not been fully exploited for data-efficient dense prediction. To address these limitations, we propose a novel cross-modal knowledge distillation framework, **xModel-KD**, for 3D point cloud segmentation. Our method exploits the complementary strengths of 2D texture and 3D geometry by learning unified per-point representations through cross-modal alignment. Specifically, we design a cross-modal fusion encoder trained with a contrastive objective that enforces feature consistency between corresponding 2D and 3D representations across multiple views. By integrating powerful pre-trained backbones with a targeted fusion strategy, the proposed framework effectively transfers appearance cues from images to geometry-aware point features. Experimental results show that cross-modal fusion achieves a 2% absolute improvement in mIoU over a LiDAR-only baseline, demonstrating the benefit of leveraging complementary multi-modal information for scalable and annotation-efficient 3D scene understanding. **Source code is available here.**

**Index Terms**—Cross-modal learning, contrastive learning, knowledge distillation, lidar perception, multi-modal fusion.

## I. INTRODUCTION

Semantic segmentation of outdoor and indoor scenes is a fundamental task for autonomous driving and robotics, enabling robust scene understanding and safe navigation [1], [2]. Recent years have witnessed remarkable progress in both camera-based methods [3], [4], [5] and LiDAR-based methods [6], [7]. While cameras provide rich appearance cues (color, texture, and fine boundaries), they lack explicit depth information and are sensitive to illumination changes.

We acknowledge that this research was enabled in part by the support of the Natural Sciences and Engineering Research Council of Canada (NSERC), DGECR/416-2022, and the support provided by the Digital Research Alliance of Canada (<https://alliancecan.ca/en>).

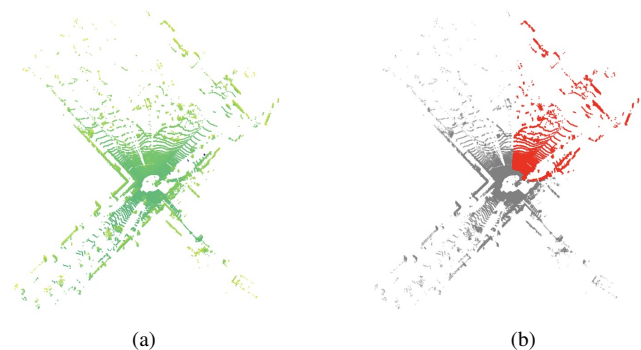


Fig. 1. Illustration of LiDAR point cloud and camera FOV. (a) Raw 360° LiDAR point cloud. (b) Camera FOV from the same scene; the red region indicates the portion of the LiDAR points visible from the camera perspective.

In contrast, LiDAR point clouds provide accurate geometric structure and robustness to environmental conditions, but lack semantic richness and exhibit non-uniform point density with increasing distance. These complementary properties have motivated emerging research on multi-modal solutions [8], [9], [10], where image features are injected into point cloud information via point-to-pixel correspondences.

Despite promising accuracy gains, existing fusion approaches face three key issues that hinder practical deployment. (i) Field-of-View (FOV) mismatch: Differences in sensing ranges between LiDAR and cameras create substantial coverage gaps (see Fig. 1). A significant portion of LiDAR points fall outside the camera’s field of view, limiting cross-modal correspondence. For instance, approximately 23.2% and 33.6% of LiDAR points are not covered by the camera FOV in the nuScenes and Waymo datasets, respectively [2], [11]. Most fusion methods discard these out-of-FOV points during training and inference [8], [12]. Discarding valuable geometric information will weaken generalization performance. (ii) Computational overhead: It poses a critical challenge for real-time systems; multi-modal inference must process both images and point clouds, introducing substantial latency and memory cost due to heavy fusion modules and transformer-based designs [9], [8]. (iii) Limited utilization of Vision Foundation Models (VFMs): While 2D vision has been transformed by large-scale pretraining [13], 3D semantic segmentation still largely relies on 3D-only architectures trained from scratch

[14], [15]. Recent attempts at 2D-to-3D transfer either rely on implicit distillation and suffer from modality gaps [10], or require extracting heavy 2D features at inference time, increasing latency and memory consumption [16].

To address these limitations, we propose `xModel-KD`, a lightweight framework that explicitly transfers rich 2D semantic knowledge from a frozen 2D teacher into a compact 3D network during training only, incurring zero inference overhead. The central idea is to decouple cross-modal learning from deployment: rather than fusing 2D features at inference, we treat the 2D model as a strong teacher and train the 3D backbone to internalize its semantic priors.

A natural question then arises: *how can 2D semantic knowledge be effectively transferred to the 3D model?* To this end, `xModel-KD` adopts a multi-scale contrastive distillation strategy. Hierarchical representations from intermediate and deep layers of the frozen 2D backbone are aligned with multi-resolution features from the 3D backbone. Lightweight projection heads map both modalities into a shared embedding space, where a contrastive objective pulls matched point-pixel pairs (via LiDAR-to-image projection) closer while pushing non-matching pairs apart.

Unlike single-layer distillation, multi-scale alignment allows the 3D network to absorb complementary 2D priors across different levels of abstraction: intermediate layers convey spatial structure and boundary cues, while deeper layers provide high-level semantic discrimination. This enriched feature hierarchy also benefits out-of-FOV points. Even without direct pixel correspondences, these points inherit stronger representations through shared 3D parameters learned under 2D supervision. At deployment, the 2D branch and all cross-modal components are removed, retaining only the enhanced 3D backbone. Consequently, `xModel-KD` delivers VFM-level semantic priors without requiring images, fusion modules, or additional memory and latency at runtime.

Our main contributions are summarized as follows:

- Proposing `xModel-KD`, a training-only cross-modal knowledge distillation framework that transfers semantic knowledge from frozen 2D teachers into 3D segmentation networks with zero inference overhead.
- Introducing a multi-scale contrastive objective to align hierarchical 2D and 3D representations, enabling effective transfer of both intermediate (boundary/structure) and deep (semantic) priors.
- Designing a lightweight and deployable learning pipeline that mitigates FOV mismatch while preserving inference efficiency by eliminating the 2D pathway at test time.

## II. RELATED WORK

Semantic segmentation for 3D scene understanding has witnessed rapid progress over the past decade, driven by advances in deep learning and the increasing availability of large-scale LiDAR and image datasets. Existing approaches can be broadly categorized into point-based, projection-based, voxel-based, camera-based, and multi-modal learning frameworks.

Each paradigm offers distinct advantages in terms of representation power, computational efficiency, and robustness, while also exhibiting inherent limitations. In this section, we review representative works across these categories and discuss their contributions and shortcomings, particularly in the context of LiDAR semantic segmentation and cross-modal learning.

### A. Point-based Methods

These methods aim to approximate a permutation-invariant set function through per-point Multi-Layer Perceptrons (MLPs). PointNet [17] pioneered this line of research, and subsequent studies have introduced point-wise MLPs [18], [19], adaptive weighting mechanisms, and pseudo-grid strategies to capture local geometric structures, while others have explored non-local operators to model long-range dependencies. However, these methods often suffer from inefficiency in LiDAR applications due to the computational cost of point sampling and grouping operations.

### B. Projection-based Methods

This category of models provides computational efficiency by projecting point clouds onto 2D representations, enabling the direct application of conventional CNNs. Common projection strategies include planar [20], [3], spherical, and hybrid projections. Nonetheless, projection inevitably leads to information loss, and these methods have reached a performance bottleneck in segmentation accuracy.

### C. Voxel-based Methods

Voxel-based approaches have recently become dominant for balancing accuracy and efficiency. Sparse Convolution [6] techniques improve upon traditional 3D CNNs by storing only non-empty voxels in hash tables and performing convolutions selectively, thus enhancing computational efficiency. Building on this idea, several advanced architectures have been proposed. Cylinder3D [15] introduces cylindrical voxels with an asymmetric network design to boost performance.

### D. Camera-based Methods

Camera-based semantic segmentation focuses on assigning pixel-level semantic labels to 2D images. The Fully Convolutional Network (FCN) [3] was the pioneering framework in this field, introducing an end-to-end convolutional architecture derived from image classification networks. Subsequent research has substantially advanced performance by incorporating multi-scale feature learning strategies [4], and attention mechanisms [5]. These approaches have significantly enhanced contextual understanding and spatial consistency in segmentation results. However, camera-only methods are inherently limited by factors such as lighting conditions, occlusions, and the absence of direct depth information, which restrict their robustness in complex real-world environments.

### E. Multi-modal Learning

This approach has emerged as a powerful paradigm by jointly exploiting the complementary strengths of RGB images and LiDAR point clouds. Early fusion-based approaches project LiDAR points onto image planes to establish point-to-pixel correspondences and inject visual features into point representations. While effective, such methods are constrained by FOV mismatch and the requirement for tightly aligned multi-modal data at inference time.

To alleviate these limitations, Yan *et al.* [10] propose 2DPASS, a training-only multi-modal distillation framework that leverages camera images as semantic priors to enhance LiDAR representations. By employing a multi-scale fusion-to-single knowledge distillation strategy, 2DPASS transfers rich 2D semantic information into a pure 3D network during training, enabling image-free inference. More recently, foundation-model-based approaches have been explored to further strengthen cross-modal learning. Knaebel *et al.* [16] introduce DINO In The Room (DITR), which injects features extracted from large-scale 2D vision foundation models into 3D segmentation backbones via 2D-to-3D feature projection. In addition, they propose a distillation variant that aligns 3D representations with frozen 2D foundation features, allowing the model to retain strong semantic priors even when images are unavailable at inference. This approach demonstrates consistent improvements across both indoor and outdoor benchmarks. Addressing robustness and modality-misalignment issues, Sun *et al.* [21] propose a Uni-to-Multi Modal Knowledge Distillation framework for bidirectional LiDAR-camera semantic segmentation. Their method introduces a bidirectional feature fusion and imputation mechanism to handle out-of-FOV points and missing image features, combined with a unimodal teacher to a multi-modal student distillation strategy.

Overall, these works highlight a growing trend toward leveraging cross-modal knowledge transfer and distillation to overcome the inherent limitations of direct fusion.

## III. METHODOLOGY

The proposed approach, as illustrated in Fig. 2 subsumes three sub-tasks: (i) multi-scale feature extraction with separate 2D and 3D encoder-decoder (EnDec) backbones, (ii) multi-scale contrastive alignment for cross-modal feature fusion, and (iii) cross-modal knowledge distillation.

### A. Multi-scale Feature Extraction

Table I provides a layer-by-layer detail of the proposed  $x_{\text{Model}}\text{-KD}$ , which processes multi-scale features hierarchically from both RGB and LiDAR inputs. The LiDAR input  $\mathbf{X} \in \mathbb{R}^{[b,p,4]}$  is processed by a 3D backbone, producing point-wise embeddings  $\mathbf{F}_{3D} \in \mathbb{R}^{[b,p,l_c]}$ , where each point is mapped to a  $l_c$ -dimensional latent feature space. In parallel, the RGB image  $\mathbf{I} \in \mathbb{R}^{[b,3,H,W]}$  is encoded using a 2D backbone, yielding spatial feature maps  $\mathbf{F}_{2D} \in \mathbb{R}^{[b,H',W',l_h]}$ , where  $l_h$  denotes the number of feature channels. To enable cross-modal alignment, the backbone features from both modalities are mapped into a shared embedding space through modality-specific projection

TABLE I  
LAYER SPECIFICATIONS OF THE PROPOSED  $x_{\text{Model}}\text{-KD}$ .

Component	Input	Output
Encoders		
LiDAR input - $\mathbf{X}$	$[b, p, 4]$	-
RGB input - $\mathbf{I}$	$[b, 3, H, W]$	-
3D Backbone (SPVCNN)	$\mathbf{X}$	$[b, p, l_c]$
2D Backbone (ResNet50)	$\mathbf{I}$	$[b, H', W', l_h]$
Projection Head		
Proj. Head - $\mathbf{Z}_{3D}$	$l_c$	$\mathbf{d}_p - 128$
Proj. Head - $\mathbf{Z}_{2D}$ (train only)	$l_h$	$\mathbf{d}_p - 128$
Contrastive Module (train only)	$(\mathbf{Z}_{3D}, \mathbf{Z}_{2D})$	$\mathcal{L}_{\text{contrast}}$
Inverse Projection		
Inverse Proj. - $\mathbf{Z}_{3D}$	$\mathbf{d}_p - 128$	$l_h$
Inverse Proj. - $\mathbf{Z}_{2D}$ (train only)	$\mathbf{d}_p - 128$	$l_c$
Decoders and Outputs		
3D Decoder	$[b, p, l_h]$	$[b, p, K]$
2D Decoder (train only)	$[b, H', W', l_c]$	$[b, H, W, K]$

Note:  $b$  - batch size;  $p$  - number of data points in each LiDAR point cloud sample;  $H, W$  - spatial dimension of the input RGB image.

heads. Specifically, the 3D features,  $\mathbf{F}_{3D} \in \mathbb{R}^{[b,p,l_c]}$  are projected to  $\mathbf{Z}_{3D} \in \mathbb{R}^{[b,p,d_p]}$ , while the 2D features  $\mathbf{F}_{2D} \in \mathbb{R}^{[b,H',W',l_h]}$  are projected to  $\mathbf{Z}_{2D} \in \mathbb{R}^{[b,H',W',d_p]}$ , where  $d_p$  denotes the projection dimension (set to 128 in this case). Thus, both the modalities are projected into the same dimensional embedding space ( $d_p$ ), ensuring that  $\mathbf{Z}_{3D}$  and  $\mathbf{Z}_{2D}$  have matching feature dimensions at each scale, which is required for contrastive alignment. Mapping both modalities into a shared  $d_p$ -dimensional space facilitates contrastive learning and cross-modal feature alignment. After cross-modal alignment in the shared embedding space, the projected features are mapped back to their respective modality-specific feature dimensions through inverse projection layers. Specifically, the aligned 3D embeddings  $\mathbf{Z}_{3D} \in \mathbb{R}^{[b,p,d_p]}$  are transformed into  $\tilde{\mathbf{F}}_{3D} \in \mathbb{R}^{[b,p,l_c]}$ , where the inverse projection restores the feature dimensionality required by the subsequent 3D decoder. Similarly, the aligned 2D embeddings  $\mathbf{Z}_{2D} \in \mathbb{R}^{[b,H',W',d_p]}$  are mapped to  $\tilde{\mathbf{F}}_{2D} \in \mathbb{R}^{[b,H',W',l_h]}$  during training. These inverse transformations allow the modality-specific decoders to operate in their corresponding feature spaces while preserving the cross-modal alignment learned in the projection space.

### B. Multi-Scale Contrastive Alignment

To establish cross-modal correspondences, as summarized in Algorithm 1 also As illustrated in Fig. 2, the dashed box denotes the multi-scale contrastive module, which is repeated across  $S$  scales to align 2D and 3D features, we employ a multi-scale contrastive learning module that aligns 2D and 3D features in a shared embedding space. At each scale  $s$ , we extract features  $f_{3D}^s$  from the 3D backbone and  $f_{2D}^s$  from the 2D backbone. These features are projected into a common embedding space using modality-specific projection heads, as defined in (1).

$$\mathbf{z}_{3D}^s = \text{Proj}_{\cdot 3D}^s(f_{3D}^s), \quad \mathbf{z}_{2D}^s = \text{Proj}_{\cdot 2D}^s(f_{2D}^s) \quad (1)$$

Using known camera-to-LiDAR calibration parameters, we establish point-to-pixel correspondence relationships. A normalized temperature-scaled cross-entropy (NT-Xent) contrastive

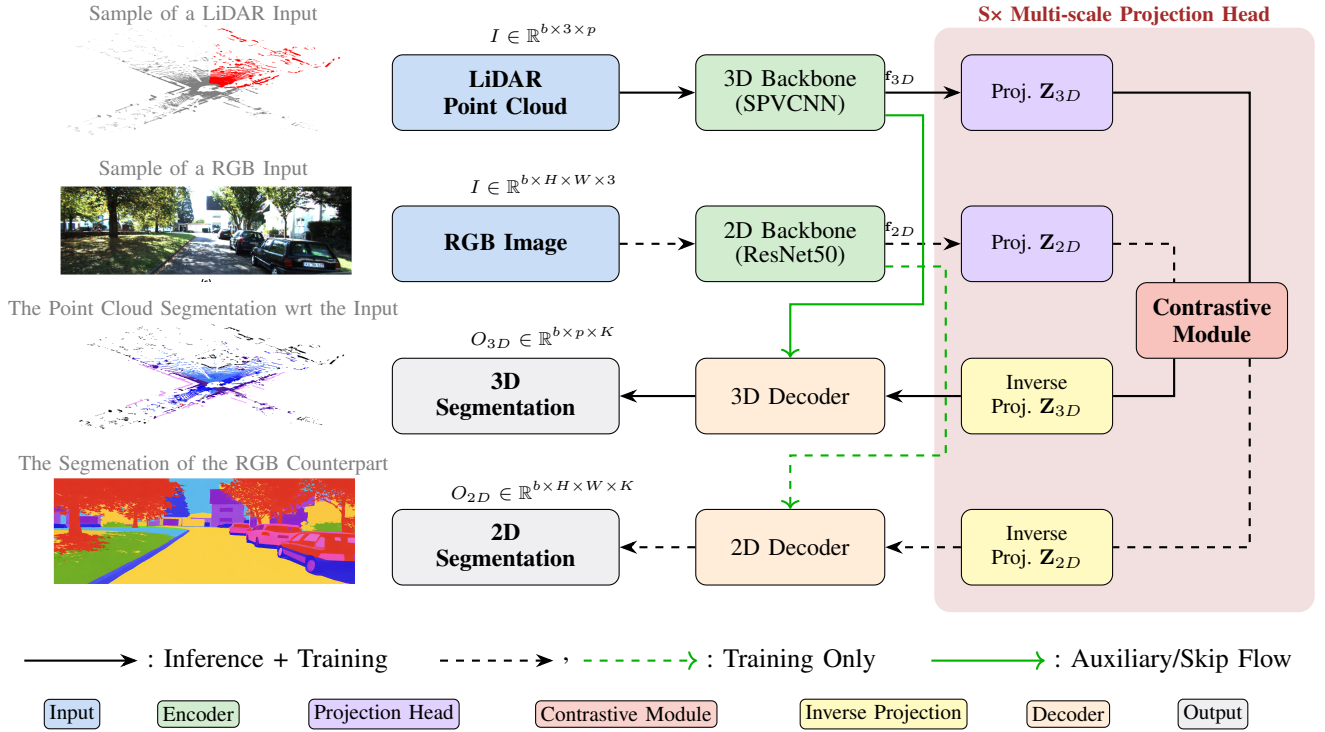


Fig. 2. Overview of the proposed  $xModel-KD$ . It jointly learns unified representations from LiDAR and RGB data using separate 3D and 2D encoders. Multi-scale features are projected into a shared embedding space and aligned via a contrastive module. The aligned features are fed into 2D and 3D decoders for simultaneous segmentation. Cross-modal distillation enforces prediction consistency during training, while only the 3D stream is used at inference.

### Algorithm 1 Multi-Scale Contrastive Alignment

**Require:**  $\{f_{3D}^s\}_{s=1}^S$ ,  $\{f_{2D}^s\}_{s=1}^S$  (multi-scale features),  $\text{Proj}_{3D}^s$ ,  $\text{Proj}_{2D}^s$  (projection heads),  $\tau$  (temperature)

**Ensure:**  $\mathcal{L}_{\text{contrast}}$  (total contrastive loss)

- 1:  $\mathcal{L}_{\text{total}} \leftarrow 0$
- 2: **for**  $s = 1$  to  $S$  **do**
- 3:  $\mathbf{z}_{3D}^s \leftarrow \text{Proj}_{3D}^s(f_{3D}^s)$  ▷ Project 3D features
- 4:  $\mathbf{z}_{2D}^s \leftarrow \text{Proj}_{2D}^s(f_{2D}^s)$  ▷ Project 2D features
- 5:  $\mathbf{z}_{3D}^s \leftarrow \text{Normalize}(\mathbf{z}_{3D}^s)$  ▷ L2 normalization
- 6:  $\mathbf{z}_{2D}^s \leftarrow \text{Normalize}(\mathbf{z}_{2D}^s)$
- 7:  $\text{logits} \leftarrow \frac{1}{\tau} \mathbf{z}_{3D}^s \cdot (\mathbf{z}_{2D}^s)^\top$  ▷ Compute similarity matrix
- 8:  $\text{labels} \leftarrow \text{arange}(N)$  ▷ Positive pairs on diagonal
- 9:  $\mathcal{L}_{\text{contrast}}^s \leftarrow \text{CrossEntropy}(\text{logits}, \text{labels})$  ▷ NT-Xent loss
- 10:  $\mathcal{L}_{\text{total}} \leftarrow \mathcal{L}_{\text{total}} + \frac{1}{S} \mathcal{L}_{\text{contrast}}^s$
- 11: **end for**
- 12: **return**  $\mathcal{L}_{\text{total}}$

loss given by (2) encourages matched pairs to have similar embeddings.

$$\mathcal{L}_{\text{contrast}}^s = -\log \frac{\exp(\text{sim}(\mathbf{z}_{3D}^s, \mathbf{z}_{2D}^s)/\tau)}{\sum_{j=1}^N \exp(\text{sim}(\mathbf{z}_{3D}^s, \mathbf{z}_{2D}^{(j)})/\tau)}, \quad (2)$$

where  $\text{sim}(a, b) = \frac{a \cdot b}{\|a\| \|b\|}$  is cosine similarity,  $\tau$  is the temperature parameter, and  $N$  is the batch size. The total contrastive loss aggregates across scales is formulated as (3)

$$\mathcal{L}_{\text{contrast}} = \frac{1}{S} \sum_{s=1}^S \mathcal{L}_{\text{contrast}}^s \quad (3)$$

Through this contrastive objective, both modalities learn mutually aligned representations that capture complementary geometric and semantic information.

### C. Cross-modal Knowledge Distillation

To maintain prediction consistency and encourage knowledge transfer between modalities, we apply the KL divergence between matched 2D pixel predictions and 3D point predictions using established point–pixel correspondences. Let  $\Omega$  denote the set of LiDAR points that fall within the camera field of view. Using known camera–LiDAR calibration parameters, each point  $i \in \Omega$  is projected to its corresponding pixel coordinate  $\pi(i)$  on the image plane. Thus, the knowledge distillation loss,  $\mathcal{L}_{\text{KD}}$ , can be calculated as in (4).

$$\mathcal{L}_{\text{KD}} = \frac{1}{|\Omega|} \sum_{i \in \Omega} \text{KL}(P_{2D}(\pi(i)) \| P_{3D}(i)), \quad (4)$$

where  $P_{3D}(i)$  denotes the predicted class distribution for LiDAR point  $i$ , computed using  $\text{softmax}(\hat{y}_{3D}(i))$  and  $P_{2D}(\pi(i))$  denotes the predicted distribution at the corresponding image pixel, estimated using  $\text{softmax}(\hat{y}_{2D}(\pi(i)))$ .

The KL divergence is, therefore, computed only over matched point–pixel pairs. Points outside the camera field of view are excluded from this loss but indirectly benefit

from shared 3D parameters optimized under matched supervision. The combination of multi-scale contrastive alignment, weighted fusion, and multi-task optimization enables the framework to learn rich, modality-aligned representations that leverage complementary geometric and semantic cues from both LiDAR and camera data, significantly improving downstream 3D semantic segmentation performance.

#### D. Loss Function Formulation

The  $xModel-KD$  is trained using a multi-task objective that jointly optimizes segmentation, cross-modal contrastive alignment, and knowledge distillation, as defined in (5).

$$\mathcal{L}_{total} = \mathcal{L}_{3D} + \mathcal{L}_{2D} + \lambda_{contrast}\mathcal{L}_{contrast} + \lambda_{KD}\mathcal{L}_{KD}, \quad (5)$$

where  $\mathcal{L}_{3D}$  and  $\mathcal{L}_{2D}$  denote the 3D and 2D segmentation losses, respectively,  $\mathcal{L}_{contrast}$  is the cross-modal contrastive loss weighted by  $\lambda_{contrast}$ , and  $\mathcal{L}_{KD}$  is the knowledge distillation loss weighted by  $\lambda_{KD}$ . Hence, the segmentation losses are:

$$\mathcal{L}_{3D} = \mathcal{L}_{CE}(\hat{y}_{3D}, y_{3D}) + \mathcal{L}_{Lovász}(\hat{y}_{3D}, y_{3D}), \quad (6)$$

$$\mathcal{L}_{2D} = \mathcal{L}_{CE}(\hat{y}_{2D}, y_{img}) + \mathcal{L}_{Lovász}(\hat{y}_{2D}, y_{img}), \quad (7)$$

where  $\hat{y}$  and  $y$  denote the predicted and ground-truth labels, respectively. The combination of cross-entropy (CE) and Lovász-Softmax (Lovász) mitigates class imbalance while improving boundary alignment.

## IV. EXPERIMENTAL SETUP AND PERFORMANCE ANALYSIS

### A. Datasets

We evaluate  $xModel-KD$  on the SemanticKITTI benchmark [1], a large-scale outdoor LiDAR semantic segmentation dataset. SemanticKITTI provides point-wise semantic labels for LiDAR scans captured with a 64-beam sensor. Following the official split, summarized in Table II, sequences 00–07 and 09–10 are used for training and sequence 08 for validation, while sequences 11–21 are used for online test evaluation. Although SemanticKITTI does not provide dense pixel-level 2D semantic annotations, we generate 2D supervision by projecting LiDAR point-wise labels onto the image plane using known camera–LiDAR calibration parameters. Specifically, each labeled 3D point is mapped to its corresponding pixel coordinate, producing sparse 2D semantic labels. These projected labels are used solely for auxiliary supervision during training and are not required at inference time.

### B. Implementation Details

The 3D backbone is SPVCNN and the 2D backbone is ResNet50 pretrained on ImageNet. We use  $S=4$  scales and feature dimension  $d_h=64$ . We train with a total batch size of 16 for 64 epochs. we use cosine learning rate decay and standard point cloud augmentations. Inference uses only the 3D stream; all 2D and cross-modal components are removed at test time. For performance evaluation, we report mean Intersection-over-Union (mIoU) as the primary metric and overall accuracy (Acc) when applicable.

### C. Quantitative Analysis

1) *Overall Performance*: Table III presents a comparative evaluation on SemanticKITTI. Compared to the LiDAR-only baseline,  $xModel-KD$  achieves improved overall performance. Among the competing methods, it ranks second behind 2DPASS [10]. In terms of model complexity, however,  $xModel-KD$  is considerably more efficient, whereas 2DPASS employs a substantially larger architecture with 45.6M parameters,  $xModel-KD$  contains only 1.93M parameters over 23× fewer parameters. This highlights a highly favorable performance–complexity trade-off. Such efficiency makes  $xModel-KD$  particularly attractive for real-world deployment scenarios, including resource-constrained and industrial environments where memory footprint, computational cost, and inference latency are critical factors

2) *Component Analysis*: An ablation study is conducted to assess the contributions of (i) multi-scale contrastive alignment, (ii) KL-divergence-based knowledge distillation. As reported in Table IV, each component provides measurable performance improvements. The complete model achieves the best overall results, outperforming the baseline by 2%.

3) *Sensitivity to Loss Weights*: To evaluate the influence of the loss weights in the multi-task objective, we conduct a sensitivity analysis on  $\lambda_{contrast}$  and  $\lambda_{KD}$ , as summarized in Table V. Recall that  $\lambda_{contrast}$  and  $\lambda_{KD}$  control the relative contribution of the cross-modal contrastive alignment loss  $\mathcal{L}_{contrast}$  and the knowledge distillation loss  $\mathcal{L}_{KD}$  in the total loss,  $\mathcal{L}_{total}$ , defined earlier in (5). The analysis shows that the  $xModel-KD$  remains stable across a wide range of weight values, indicating that performance is not overly sensitive to precise tuning. Optimal performance is achieved with 0.1 set for both  $\lambda_{contrast}$  and  $\lambda_{KD}$ , demonstrating that both contrastive alignment and knowledge distillation contribute meaningfully.

### D. Qualitative Results

Fig. 3 presents qualitative comparisons between the ground truth and our model predictions in the bird’s-eye view (BEV) on the SemanticKITTI validation set. The results show that our model produces predictions that closely match the ground truth, demonstrating accurate semantic segmentation performance. In particular, the predicted regions exhibit consistent spatial structures. These qualitative observations are consistent with the quantitative results, further confirming the effectiveness of our approach.

## V. CONCLUSION

The proposed  $xModel-KD$ , a training-only cross-modal knowledge distillation framework for LiDAR semantic segmentation that transfers rich semantic priors from a frozen 2D teacher into a compact 3D backbone while preserving zero inference overhead. Unlike conventional multi-modal fusion methods that require images and heavy fusion modules at test time,  $xModel-KD$  decouples cross-modal learning from deployment by leveraging multi-scale contrastive alignment and KL-based distillation during training only.



TABLE IV

ABLATION STUDY ON THE SEMANTICKITTI VALIDATION SET.  
NOTE: ✓ - INCLUDED, ✗ - OMITTED

Configuration	MSCA	KD	mIoU (%)
Baseline (LiDAR only)	✗	✗	67.0
+ Contrastive	✓	✗	67.8
+ KL-divergence + Contrastive	✓	✗	68.4
xModel-KD	✓	✓	69.1

TABLE V

SENSITIVITY ANALYSIS OF WEIGHT PARAMETERS IN THE MULTIMODAL LOSS USED FOR xMODEL-KD

$\lambda_{\text{contrast}}$	$\lambda_{\text{KD}}$	mIoU (%)	Acc (%)
0.05	0.05	68.2	92.6
0.10	0.05	68.7	92.8
0.10	0.10	69.0	93.0
0.20	0.10	68.8	92.9

Extensive experiments on SemanticKITTI demonstrate that xModel-KD consistently performs across various object classes. Beyond accuracy improvements, xModel-KD is lightweight in terms of parameters and computational complexity, making it suitable for real-time deployment on resource-constrained platforms. This efficiency, combined with LiDAR-only inference, makes the framework particularly attractive for practical applications such as autonomous systems, warehouse robotics, and indoor industrial inspection. Nevertheless, it relies on accurate LiDAR-camera calibration and point-pixel correspondences during training, and its generalization to strongly misaligned or degraded sensor conditions requires further investigation. Overall, xModel-KD demonstrates that training-time cross-modal knowledge transfer is an effective and deployment-efficient strategy for enhancing 3D semantic segmentation without sacrificing inference efficiency.

## REFERENCES

- [1] J. Behley, M. Garbade, A. Milioto, J. Quenzel, S. Behnke, C. Stachniss, and J. Gall, "Semantickitti: A dataset for semantic scene understanding of lidar sequences," in *Proceedings of the IEEE/CVF international conf. on computer vision*, 2019, pp. 9297–9307.
- [2] H. Caesar, V. Bankiti, A. H. Lang, S. Vora, V. E. Liong, Q. Xu, A. Krishnan, Y. Pan, G. Baldan, and O. Beijbom, "nuscenes: A multimodal dataset for autonomous driving," in *Proceedings of the IEEE/CVF conf. on computer vision and pattern recognition*, 2020, pp. 11 621–11 631.
- [3] W. Wu, Z. Qi, and L. Fuxin, "Pointconv: Deep convolutional networks on 3d point clouds," in *Proceedings of the IEEE/CVF conf. on computer vision and pattern recognition*, 2019, pp. 9621–9630.
- [4] G. Lin, C. Shen, A. Van Den Hengel, and I. Reid, "Efficient piecewise training of deep structured models for semantic segmentation," in *Proceedings of the IEEE conf. on computer vision and pattern recognition*, 2016, pp. 3194–3203.
- [5] Z. Huang, X. Wang, L. Huang, C. Huang, Y. Wei, and W. Liu, "Ccnet: Criss-cross attention for semantic segmentation," in *Proceedings of the IEEE/CVF international conf. on computer vision*, 2019, pp. 603–612.
- [6] H. Tang, Z. Liu, S. Zhao, Y. Lin, J. Lin, H. Wang, and S. Han, "Searching efficient 3d architectures with sparse point-voxel convolution," in *European conf. on computer vision*. Springer, 2020, pp. 685–702.
- [7] X. Zhu, H. Zhou, T. Wang, F. Hong, Y. Ma, W. Li, H. Li, and D. Lin, "Cylindrical and asymmetrical 3d convolution networks for lidar segmentation," in *Proceedings of the IEEE/CVF conf. on computer vision and pattern recognition*, 2021, pp. 9939–9948.
- [8] Z. Zhuang, R. Li, K. Jia, Q. Wang, Y. Li, and M. Tan, "Perception-aware multi-sensor fusion for 3d lidar semantic segmentation," in *Proceedings of the IEEE/CVF international conf. on computer vision*, 2021, pp. 16 280–16 290.
- [9] J. Li, H. Dai, H. Han, and Y. Ding, "Mseg3d: Multi-modal 3d semantic segmentation for autonomous driving," in *Proceedings of the IEEE/CVF conf. on computer vision and pattern recognition*, 2023, pp. 21 694–21 704.
- [10] X. Yan, J. Gao, C. Zheng, C. Zheng, R. Zhang, S. Cui, and Z. Li, "2dpas: 2d priors assisted semantic segmentation on lidar point clouds," in *European conf. on computer vision*. Springer, 2022, pp. 677–695.
- [11] P. Sun, H. Kretzschmar, X. Dotiwalla, A. Chouard, V. Patnaik, P. Tsui, J. Guo, Y. Zhou, Y. Chai, B. Caine *et al.*, "Scalability in perception for autonomous driving: Waymo open dataset," in *Proceedings of the IEEE/CVF conf. on computer vision and pattern recognition*, 2020, pp. 2446–2454.
- [12] T. Huang, Z. Liu, X. Chen, and X. Bai, "Epnet: Enhancing point features with image semantics for 3d object detection," in *European conf. on computer vision*. Springer, 2020, pp. 35–52.
- [13] M. Oquab, T. Darcet, T. Moutakanni, H. Vo, M. Szafraniec, V. Khalidov, P. Fernandez, D. Haziza, F. Massa, A. El-Nouby *et al.*, "Dinov2: Learning robust visual features without supervision," *Transactions on Machine Learning Research Journal*, pp. 1–31, 2024.
- [14] X. Wu, L. Jiang, P.-S. Wang, Z. Liu, X. Liu, Y. Qiao, W. Ouyang, T. He, and H. Zhao, "Point transformer v3: Simpler faster stronger," in *Proceedings of the IEEE/CVF conf. on computer vision and pattern recognition*, 2024, pp. 4840–4851.
- [15] H. Zhou, X. Zhu, X. Song, Y. Ma, Z. Wang, H. Li, and D. Lin, "Cylinder3d: An effective 3d framework for driving-scene lidar semantic segmentation," *arXiv preprint arXiv:2008.01550*, 2020.
- [16] K. Abou Zeid, K. Yilmaz, D. de Geus, A. Hermans, D. B. Adrian, T. Linder, and B. Leibe, "Dino in the room: Leveraging 2d foundation models for 3d segmentation," in *Thirteenth International conf. on 3D Vision*, 2025.
- [17] C. R. Qi, H. Su, K. Mo, and L. J. Guibas, "Pointnet: Deep learning on point sets for 3d classification and segmentation," in *Proceedings of the IEEE conf. on computer vision and pattern recognition*, 2017, pp. 652–660.
- [18] C. R. Qi, L. Yi, H. Su, and L. J. Guibas, "Pointnet++: Deep hierarchical feature learning on point sets in a metric space," *Advances in neural information processing systems*, vol. 30, 2017.
- [19] Y. Wang, Y. Sun, Z. Liu, S. E. Sarma, M. M. Bronstein, and J. M. Solomon, "Dynamic graph cnn for learning on point clouds," *ACM Transactions on Graphics (tog)*, vol. 38, no. 5, pp. 1–12, 2019.
- [20] F. J. Lawin, M. Danelljan, P. Tosteberg, G. Bhat, F. S. Khan, and M. Felsberg, "Deep projective 3d semantic segmentation," in *International conf. on computer analysis of images and patterns*. Springer, 2017, pp. 95–107.
- [21] T. Sun, Z. Zhang, X. Tan, Y. Peng, Y. Qu, and Y. Xie, "Uni-to-multi modal knowledge distillation for bidirectional lidar-camera semantic segmentation," *IEEE Transactions on Pattern Analysis and Machine Intelligence*, vol. 46, no. 12, pp. 11 059–11 072, 2024.
- [22] B. Wu, X. Zhou, S. Zhao, X. Yue, and K. Keutzer, "Squeezesegv2: Improved model structure and unsupervised domain adaptation for road-object segmentation from a lidar point cloud," in *international conf. on robotics and automation (ICRA)*. IEEE, 2019, pp. 4376–4382.
- [23] A. Milioto, I. Vizzo, J. Behley, and C. Stachniss, "Rangenet++: Fast and accurate lidar semantic segmentation," in *2019 IEEE/RSJ international conf. on intelligent robots and systems (IROS)*. IEEE, 2019, pp. 4213–4220.
- [24] Q. Hu, B. Yang, L. Xie, S. Rosa, Y. Guo, Z. Wang, N. Trigoni, and A. Markham, "Randla-net: Efficient semantic segmentation of large-scale point clouds," in *Proceedings of the IEEE/CVF conf. on computer vision and pattern recognition*, 2020, pp. 11 108–11 117.
- [25] H. Thomas, C. R. Qi, J.-E. Deschaud, B. Marcotegui, F. Goulette, and L. J. Guibas, "Kpconv: Flexible and deformable convolution for point clouds," in *Proceedings of the IEEE/CVF international conf. on computer vision*, 2019, pp. 6411–6420.
- [26] J. Xu, R. Zhang, J. Dou, Y. Zhu, J. Sun, and S. Pu, "Rpvnet: A deep and efficient range-point-voxel fusion network for lidar point cloud segmentation," in *Proceedings of the IEEE/CVF international conf. on computer vision*, 2021, pp. 16 024–16 033.